Rare Metal Materials and Engineering
Volume 52, Issue 5, May 2023
Available online at www.rmme.ac.cn

Science Press

Cite this article as: Wang Tao, Ding Yutian, Wang Xingmao, et al. Microstructure and Texture Evolution of Ni-based Superalloy During Deformation and Thermomechanical Treatments[J]. Rare Metal Materials and Engineering, 2023, 52(05): 1555-1564.

ARTICLE

Microstructure and Texture Evolution of Ni-based Superalloy During Deformation and Thermomechanical Treatments

Wang Tao[1,2], Ding Yutian[1,2], Wang Xingmao[1,2,3], Gao Yubi[1,2], Bi Zhongnan[3], Du Jinhui[3], Gan Bin[3]

[1] State Key Laboratory of Advanced Processing and Recycling of Nonferrous Metals, Lanzhou University of Technology, Lanzhou 730050, China; [2] School of Materials Science and Engineering, Lanzhou University of Technology, Lanzhou 730050, China; [3] Beijing Key Laboratory of Advanced High Temperature Materials, Central Iron and Steel Research Institute, Beijing 100081, China

Abstract: The microstructure evolution, grain boundary character distribution, strain distribution, and texture evolution of Ni-based superalloy during cold rolling and subsequent recrystallization annealing treatments were studied by electron back-scattered diffraction technique. Results show that when the cold deformation degree is small ($\varepsilon \leqslant 45\%$), the grains are elongated along the rolling direction into a flat shape and distributed evenly in the matrix. The strain is mainly concentrated near the grain boundary and the twin boundary (TB), and the high-angle grain boundaries (HAGBs) and TBs are gradually transformed into sub-grain boundaries (Sub-GBs) and low-angle grain boundaries (LAGBs). Meanwhile, the Goss texture {110}<001>, Brass-R texture {111}<112>, Twinned-Copper texture {552}<115>, and Copper texture {112}<111> appear. When the rolling reduction exceeds 70%, the grain shape gradually changes from flat to fibrous, the deformation uniformity of the grains gradually becomes better, the strain distribution becomes uniform, and LAGBs begin to dominate. In addition, the texture types do not change, but the texture intensity increases. After the annealing at 1120 °C for 15 min, the length fraction of annealing twins is increased with increasing the rolling reduction. Besides, the deformation textures are transformed into the recrystallization textures, the texture types are increased, but the texture intensity weakens. Furthermore, the Copper texture {112}<111> is continuously transformed into the Twinned-Copper texture {552}<115> when the proportion of annealing twins increases. Additionally, the {124}<211> texture is generated in the as-annealed alloy after rolling reduction of 30%–80%.

Key words: Ni-based superalloy; cold rolling; annealing twins; grain boundary character distribution; texture evolution

Superalloys, usually containing iron, nickel, and cobalt, are commonly served under high temperature of above 600 °C and complex stress conditions, and they have good oxidation and corrosion resistance, good fatigue performance, and excellent fracture toughness[1–2]. Therefore, superalloys attract much attention as hot-end components and high-temperature anti-corrosion components in the fields of aviation, aerospace, and gas turbines[3–5]. Currently, Ni-based superalloys account for 80% among various superalloys[6]. The alloying method can effectively improve the mechanical properties of Ni-based superalloys. However, the addition of solid solution or precipitation strengthening elements may reduce the hot working windows, thus degrading the processing properties of alloys[7] and seriously reducing the production efficiency and quality. With the development of grain boundary engineering, the face-centered cubic metals with medium and low stacking fault energy can easily form stacking faults during the plastic deformation. When the stacking faults expand, the cross-slip of dislocations is suppressed, which promotes the twinning deformation and the formation of massive deformation twins[8–10]. During the recrystallization annealing, a large number of annealing twins with high angle grain boundaries (HAGBs) and low energy are produced in the cold-deformed alloys. Increasing the HAGB proportion and ameliorating the HAGB distribution can improve the mechanical properties of superalloys[11–12]. The microstructure evolution of superalloys

Received date: September 07, 2022
Foundation item: National Key Research and Development Program of China (2017YFA0700703).
Corresponding author: Ding Yutian, Ph. D., Professor, State Key Laboratory of Advanced Processing and Recycling of Nonferrous Metals, Lanzhou University of Technology, Lanzhou 730050, P. R. China, E-mail: dingyt@lut.edu.cn

during deformation process can be quantitatively reflected by the texture characteristics[13–17], which is conducive to the microstructure design and the enhancement in the properties of Ni-based superalloys[18]. Therefore, it is of great significance to study the evolution of microstructures and textures during cold rolling (CR) and recrystallization annealing of Ni-based superalloys.

The regulation of special grain boundaries and related textures transitions has been widely researched. Xia et al[19] proved that the proportion of special grain boundaries in 690 alloy can be effectively increased by CR and annealing. Introducing the components, such as interfaces, to form special interface microstructures can also effectively ameliorate the material properties. Zheng et al[20] reported that the interfaces play an extremely important role in the plastic deformation and mechanical behavior of nanocomposites. Wang et al[21] introduced the high-density annealing twin boundaries (TBs) into GH3625 alloy through CR and subsequent heat treatment, which greatly improved the mechanical properties of alloy. Gao[22] and Giannuzzi[23] et al studied the annealing twins in GH3625 alloy during stretching by in-situ electron back-scattered diffraction (EBSD) and ex-situ transmission electron microscope (TEM) methods. It is reported that the special grain boundaries can improve the mechanical properties of alloys, and the distribution of grain boundary character can mainly be optimized by annealing twins associated with $\Sigma 3^n$ grain boundaries, rather than the deformation twins. Gao et al[24] studied the microstructure of GH3625 alloy after CR and annealing, and found that the recrystallization process can affect the transformation of microstructures and textures. Current researches mainly focus on the texture evolution in the late stage of thermal deformation during the annealing process. Therefore, in this research, the evolution of microstructure and texture of Ni-based superalloys was jointly investigated for comprehensive analysis.

Cold deformation and subsequent heat treatment were conducted for the Ni-based superalloys in this research. The effect of CR and subsequent heat treatment on the microstructure evolution, the grain boundary character distribution, and texture evolution of the Ni-based superalloy was discussed by EBSD technique, which provided guidance for the optimization design of the CR process of Ni-based alloy sheets.

1 Experiment

The Ni-based superalloy was cast into ingots by the vacuum induction melting and electroslag remelting, and the ingots were forged into the bars (Φ150 mm) after homogenization treatment. The chemical composition of Ni-based superalloy was Ni-19.5Co-16.5Cr-5.0W-2.5Al-2.5Ti-2.5Nb-0.02C (wt%). The plate specimens (100 mm×30 mm×10 mm) were cut from the bar by wire cutting, then processed by solution treatment at 1080 °C for 2 h, and finally water-cooled (WC) to room temperature. CR with different reductions (ε=30%, 45%, 70%, 80%) was conducted by a double wheel CR mill at room temperature. Then, CR specimens were subjected to annealing treatment (AT) under the conditions of 1120 °C/15 min/WC. Table 1 shows the detailed thermomechanical treatment conditions.

The cold-deformed and annealed specimens were cut by a wire cutting machine, then mechanically ground, polished, and finally electropolished in a mixed solution of 80 mL CH_3OH+20 mL H_2SO_4 at voltage of 20 V for 6 s. Afterwards, EBSD tests were conducted, and Channel 5 software was used to analyze the average grain size, twin content, stress distribution, and texture evolution.

2 Results and Discussion

2.1 Solid solution microstructure

Fig. 1 shows the inverse pole figure (IPF) map, grain boundary character distribution map, distribution of grain boundary misorientation angle, and grain size distribution of the Ni-based superalloy after solution treatment at 1080 °C/2 h/WC. The gray lines represent the low angle grain boundaries (LAGBs, $2°<\theta<15°$), the black lines represent HAGBs ($\theta \geqslant 15°$), and the red lines represent TBs. According to Fig.1a–1b, the microstructures of ST specimen are composed of uniform and undirected equiaxed grains and a large number of annealing twins. Moreover, the annealing twins are linearly distributed in the grain interior. The annealing twins forming at the intersection angle of grain boundaries and throughout the whole grain are distinguished as type A and type B annealing twins, respectively. The annealing twins with one end inside the grain and the other end outside the grain are named as type C annealing twins[22]. It is clear that a large number of grain boundaries (27.81%) in ST specimen have the misorientation angle of near 60°. This is because the Ni-based superalloys have face-centered cubic structure with low stacking fault energy. The twin crystal plane is {111}, and the annealing twins have a misorientation relationship of 60° <111> with the γ matrix. This structure is consistent with the $\Sigma 3$ lattice, which results in the largest proportion of misorientation angle of near 60° in Fig.1c[9,23]. Fig.1d shows the grain size distribution. The average grain size with twins is d_{eff}, and that without twins is

Table 1 Detailed treatment parameters of different specimens

Specimen	Treatment
ST	Solid solution treatment
CR-30%	CR reduction of 30%
CR-45%	CR reduction of 45%
CR-70%	CR reduction of 70%
CR-80%	CR reduction of 80%
CR-30%-AT-1120-15	CR reduction of 30%+AT at 1120 °C for 15 min
CR-45%-AT-1120-15	CR reduction of 45%+AT at 1120 °C for 15 min
CR-70%-AT-1120-15	CR reduction of 70%+AT at 1120 °C for 15 min
CR-80%-AT-1120-15	CR reduction of 80%+AT at 1120 °C for 15 min

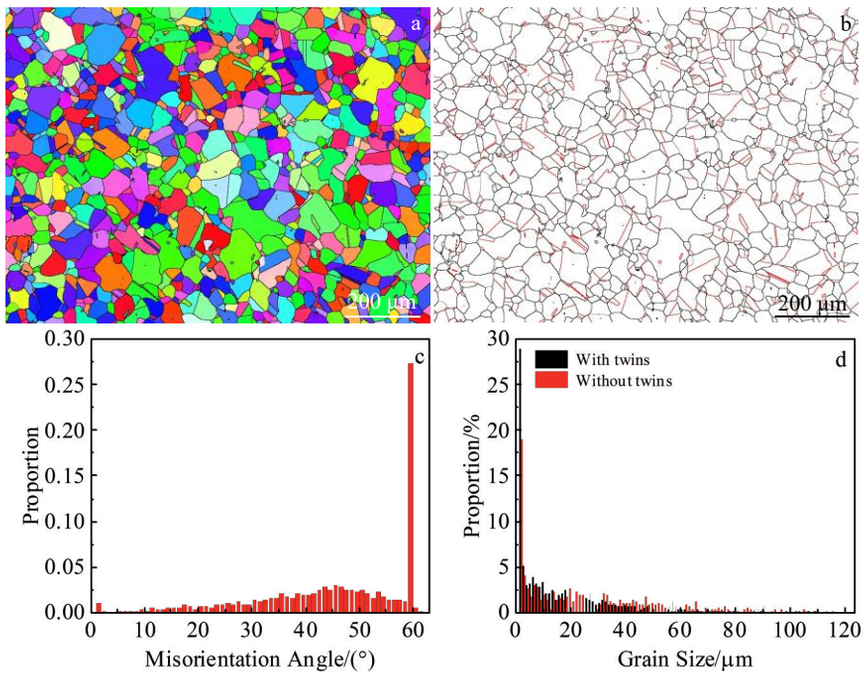

Fig.1 IPF map (a), grain boundary character distribution map (b), misorientation angle distribution (c), and grain size distribution (d) of Ni-based superalloy after solid solution treatment

d. According to Fig.1d, d_{eff}=16.59 μm and *d*=27.15 μm, which indicates that the annealing TBS and ordinary HABGs have similar grain refinement effects, and the degree of grain refinement is related to the proportion of annealing twins.

2.2 CR treatment

The microstructures change significantly when the Ni-based superalloy is cold-rolled at room temperature with different CR reductions. Lattice distortion, vacancies, and massive dislocations can result in the deformed structures, such as sub-structures and deformation twins, thereby increasing the resistance against the dislocation movement[25]. The strain distributions of the cold-rolled Ni-based superalloys are shown in Fig. 2. Different colors represent different strain distribution states, where the blue area denotes the low strain zone and the red area denotes the high strain zone. With increasing the CR reduction from 30% to 45%, the grains are elongated along the rolling direction, and the low strain regions are mainly distributed in the crystal. Nevertheless, the high strain regions are mainly distributed near the grain boundary, which is caused by the uneven rolling deformation. When the CR reduction exceeds 70%, the green spots with concentrated strain expand, becoming uniformly distributed green areas. Additionally, the green areas gradually change to red areas. The grains gradually change from flat to fibrous shape, the deformation uniformity of grains becomes better, and the concentrated strain gradually changes to the strain with uniform distribution[24]. This is because the crystallographic orientation of every grain is different in polycrystalline materials. Therefore, all grains are randomly distributed. When the polycrystal is subjected to a certain external force, the shear stress of different grains in each slip system varies greatly, which leads to the lagging occurrence of plastic deformation of grains. Generally, the grains always slip preferentially along the soft orientation, but the surrounding grains in the hard orientation are inactivated. Thus, the dislocations are blocked at the grain boundaries, and the

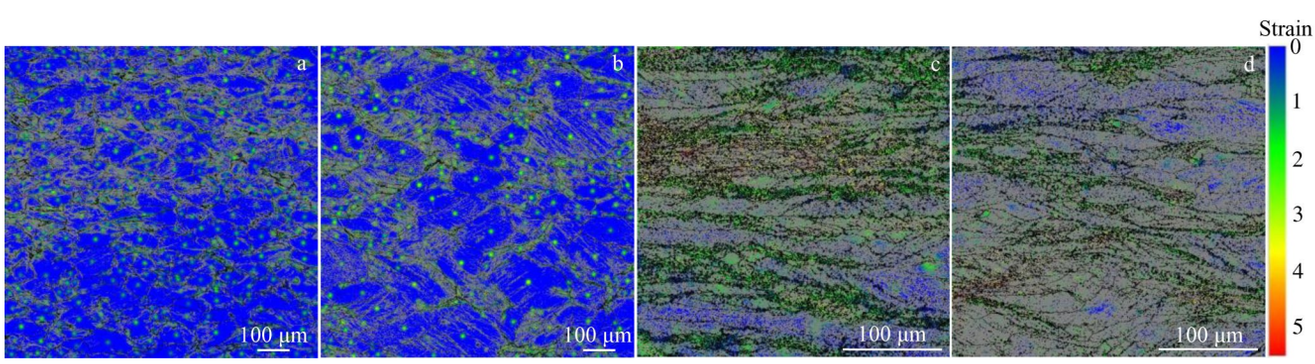

Fig.2 Strain distributions of Ni-based superalloys after cold rolling with different reductions: (a) ε=30%; (b) ε=45%; (c) ε=70%; (d) ε=80%

dislocation plugging occurs at the obstacles (grain boundaries), thereby producing a large stress concentration near the grain boundary[25–26]. With increasing the CR reduction, the dislocations are constantly plugged at obstacles (grain boundaries), and the stress concentration is increased consequently. When the stress reaches a critical value, the grains begin to slip along the hard orientation[24,27–28]. Therefore, the plastic deformation is transferred from one grain to another, and the deformation uniformity of the grains is gradually improved. EBSD data of CR specimens were imported into Channel 5 software to analyze the grain size, and the grain size results are as follows: $d_{CR\text{-}30\%}$=3.58 μm, $d_{CR\text{-}45\%}$=3.40 μm, $d_{CR\text{-}70\%}$=1.21 μm, and $d_{CR\text{-}80\%}$=1.08 μm. It is clear that the grain size is obviously refined with increasing the deformation degree. Meanwhile, with improving the grain refinement, the non-uniformity degree of grain is decreased[29].

2.3 Effect of AT and evolution of grain boundary character distribution

Fig. 3 shows the grain boundary character distribution in different Ni-based superalloys. It can be seen that the microstructures of CR specimens after annealing treatment (1120 °C/15 min/WC) are composed of randomly oriented equiaxed grains and a large number of annealing twins of type A, type B, and type C[30]. This is mainly because the deformed microstructure undergoes recovery and recrystallization, and the grains grow through the migration of grain boundaries during AT. During the migration of grain boundaries, the coherent twin boundaries are generated due to the (111) plane of atomic dense distribution, which accidently disarranges the stacking sequence. During TB migration, the annealing twins appear[9]. As the special HAGB, TBs act as the grain boundary to divide and refine grains. Besides, the twin interfaces can also provide abundant dislocation storage space to ensure sufficient work hardening and stable plastic deformation of the alloys[31–32].

Fig. 4 shows the grain size distributions of different Ni-based superalloys. Combined with Fig. 1d, it can be seen that the grain size range of annealed alloy is narrower than that of

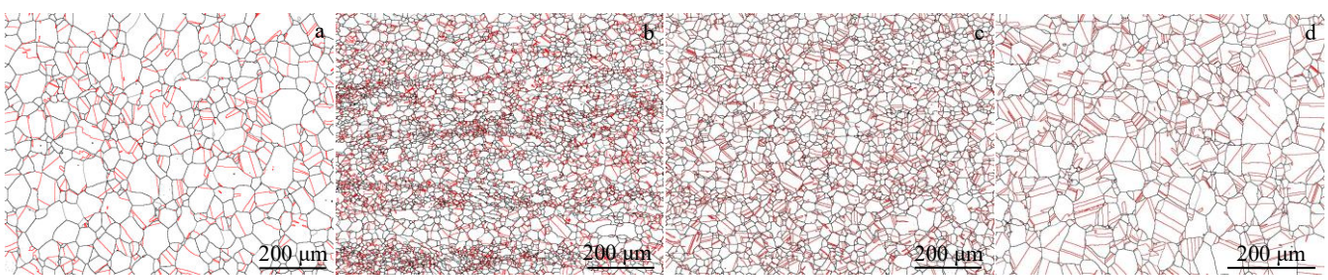

Fig.3 Grain boundary character distributions of CR-30%-AT-1120-15 (a), CR-45%-AT-1120-15 (b), CR-70%-AT-1120-15 (c), and CR-80%-AT-1120-15 (d) Ni-based superalloys

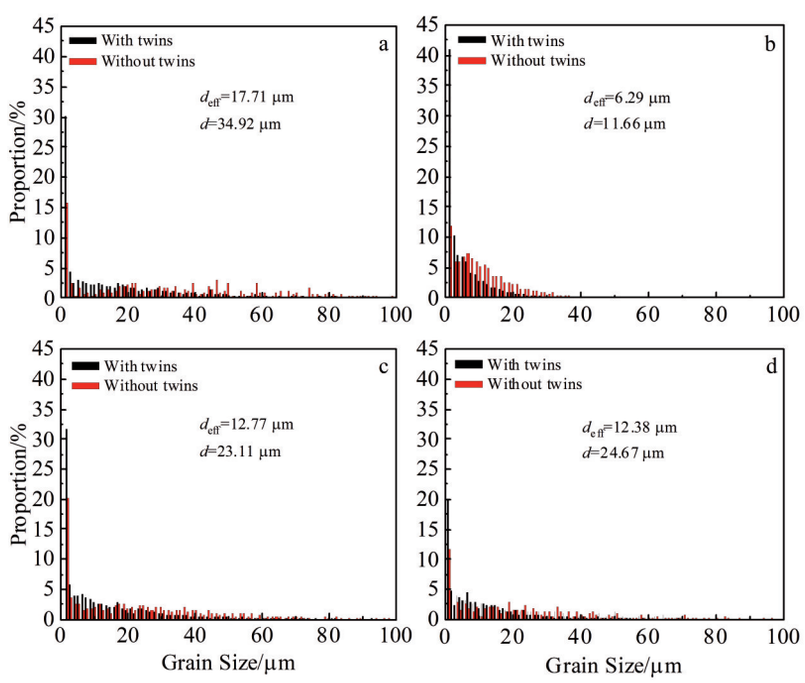

Fig.4 Grain size distributions of CR-30%-AT-1120-15 (a), CR-45%-AT-1120-15 (b), CR-70%-AT-1120-15 (c), and CR-80%-AT-1120-15 (d) Ni-based superalloys

ST specimen. In addition, the size range of grains containing twins is narrower than that without twins. The analysis shows that the refinement of grain size is closely related to the content of annealing twins, because they have the grain refinement effect. Besides, the migration rate of TBs is relatively low due to their low energy and high stability which hinder the grain growth[33]. However, the driving force for the formation of recrystallized grains in different grains during AT is different due to the uneven strain distribution in CR specimen (Fig. 2), which eventually leads to the change in grain size during the recrystallization process (Fig. 3). However, the increase in TB proportion leads to the decrease in energy of the grain boundaries, which reduces the migration distance and migration rate of the grain boundaries, even to zero. Thus, the grain boundary structure is relatively stable[34]. The ternary grain boundaries containing annealing TBs in the alloy structure can also hinder the grain growth[35]. Therefore, the grain size of CR-80%-AT-1120-15 specimen grows slowly (Fig.4d). In conclusion, the grain refinement is mainly caused by the recrystallization and the refinement of twin grains.

To describe the evolution of grain boundary character distribution of Ni-based superalloys after CR and subsequent ATs, the contents of different grain boundary characters were analyzed, as shown in Fig. 5. The deformation degree and the stored energy can be quantitively revealed by LAGBs proportion[36]. Sub-grain boundaries (Sub-GBs) indicate the grain boundaries with misorientation angle of $\theta \leqslant 2°$, LAGBs indicate the misorientation angle of $2° < \theta < 15°$, HAGBs indicate the misorientation angle of $\theta \geqslant 15°$, and TBs are special HAGBs with the ideal 60° <111> misorientation[21]. According to Fig. 5, the microstructure of ST specimen is mainly composed of 96.12% HAGBs, containing 27.81% TBs. The Sub-GBs and LAGBs account for 1.03% and 2.85%, respectively. When the ST specimen is subjected to CR, Sub-GBs and LAGBs increase significantly, whereas HAGBs and TBs decrease significantly. With increasing the CR reduction, LAGBs show an increasing trend. After the deformed

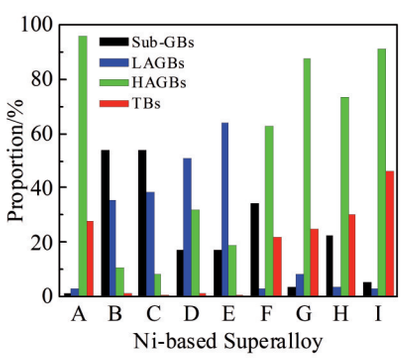

Fig.5 Grain boundary character distribution in different Ni-based superalloys (A: ST specimen; B: CR-30% specimen; C: CR-45% specimen; D: CR-70% specimen; E: CR-80% specimen; F: CR-30%-AT-1120-15 specimen; G: CR-45%-AT-1120-15 specimen; H: CR-70%-AT-1120-15 specimen; I: CR-80%-AT-1120-15 specimen)

microstructure undergoes AT at 1120 °C for 15 min, Sub-GBs and LAGBs are significantly reduced, and the HAGBs and TBs are significantly increased. With increasing the CR reduction, TBs proportion is gradually increased. Sub-GBs and LAGBs correspond to the dislocation boundary formed by the dislocation entanglements[37], whereas HAGBs and TBs correspond to the low dislocation density regions[38]. A large number of dislocations are generated in ST specimen during plastic deformation. When the dislocations move to the grain boundaries, they are blocked and the slipping is suppressed. Then, the dislocations interact with the grain boundaries and TBs. Ultimately, the proportion of HAGBs and TBs decreases and that of Sub-GBs and LAGBs increases.

However, with increasing the CR reduction, the activated slip system is increased, and the number of slip dislocations is also increased. Thus, the formation of LAGBs increases, and LAGBs are in the dominant position in CR alloy. When the deformed microstructures are annealed, the recovery and recrystallization processes occur accompanied by the annihilation of dislocations. During AT, a large number of Sub-GBs serve as the nucleation sites of new grains, and the storage energy induced by CR provides the driving force for the nucleation of recrystallized grains[21,39]. Therefore, Sub-GBs and LAGBs are gradually transformed into HAGBs and TBs, and finally the HAGBs and TBs are the dominant grain boundaries in the annealed specimens.

2.4 Texture evolution

Generally, each grain has a crystallographic orientation which is different from the orientation of adjacent grains in polycrystalline materials. Thus, all grains are randomly distributed. However, when the polycrystal undergoes plastic deformation, with increasing the CR reduction, the slip direction of different grains gradually changes into the direction of the main deformation. Therefore, a certain regularity in grain arrangement occurs in polycrystalline materials. The resultant direction is regarded as the preferred orientation, and this organization is called as the deformation texture[40–41]. The pole figures and IPFs can only provide the qualitative analysis of texture. Therefore, it is necessary to establish an orientation distribution function (ODF) method to describe the orientation distribution of polycrystals in three-dimensional space for quantitative analysis of textures. Fig. 6 shows the common orientation of space cross-section in the cubic crystal system[42]. Fig.6a–6c show the main texture types and relative positions on ODF cross-section with Euler angles of φ_2=0°, φ_2=45°, and φ_2=65°, respectively.

Fig. 7 shows the main texture types of ST specimen. Combined with Fig. 6, it can be seen that in the interface diagram with φ_2=0°, the Goss texture {110} <001>, Brass texture {110}<112>, and Brass texture {110}<110> appear along the α orientation line; Rotated-Cube texture {001}<110> appears along the θ orientation line; Brass-R texture {111} <112> appears along the γ orientation line. In the cross-section with φ_2=45°, Goss texture {110} <001> appears along the τ orientation line; Copper texture {112}<111>, Brass-R texture {111} <112>, Rotated-Cube texture {001} <110>, and

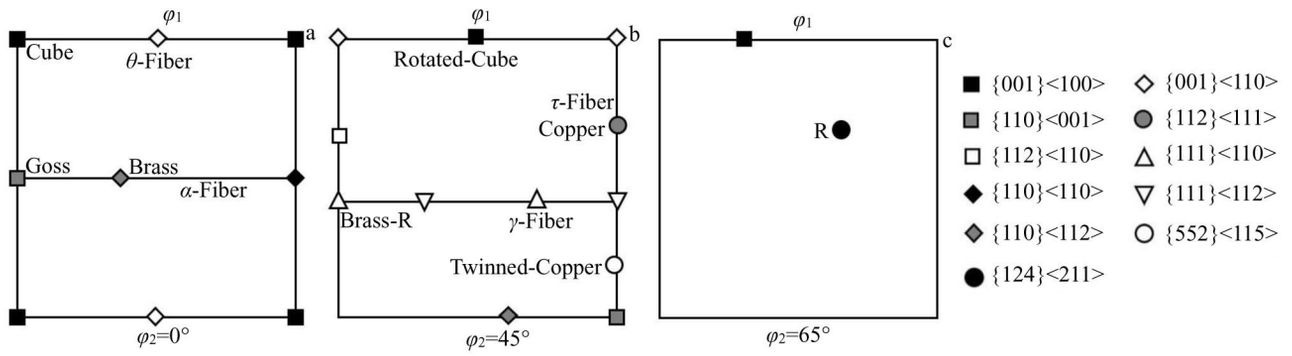

Fig.6 Common orientations on space cross-section of cubic crystals with different Eular angles: (a) φ_2=0°; (b) φ_2=45°; (c) φ_2=65° (Euler angles of φ_1, φ_2, and Φ are independent of each other) [42]

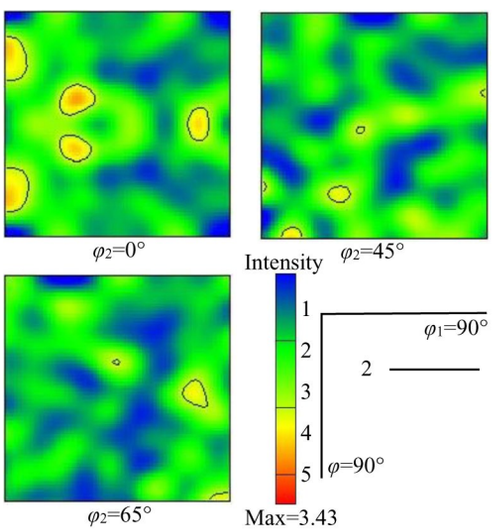

Fig.7 ODF sections of Ni-based superalloy after ST process

Twinned-Copper texture {552} <115> also appear. The recrystallization texture is the basis of plastic deformation of Ni-based superalloys during CR[13–16].

Fig. 8 shows the texture evolutions of different Ni-based superalloys. It can be seen that when φ_2=0°, Goss texture {110}<001> appears only along the α orientation line. When φ_2=45°, the Brass-R texture {111}<112> appears along the γ orientation line, and its intensity is gradually increased with increasing the CR reduction. Goss texture {110} <001>, Twinned-Copper texture {552} <115>, and Copper texture {112}<111> appear along the τ orientation line, and with increasing the CR reduction, the Copper texture {112}<111> is strengthened. When ε=45%, the strength of Copper texture {112}<111> is the strongest. With further increasing the CR reduction, the Copper texture {112}<111> gradually weakens and even disappears. Compared with that of ST specimen, the strength of Twinned-Copper texture {552} <115> decreases obviously, because the annealing twins are transformed into LAGBs and Sub-GBs during plastic deformation. However, the Twinned-Copper texture {552}<115> is increased slightly with increasing CR reduction. This is because more deformation twins are generated with increasing the CR reduction. When CR reduction is small, the Ni-based superalloy deforms in the form of dislocation slip. Because the texture can slightly restrict the plastic fluidity under deformation conditions, the Copper texture {112}<111> appears during CR[43]. When CR reduction exceeds 70%, the grain uniformity becomes better. When the grains with Copper texture {112}<111> are subject to twinning deformation (ε=70% and ε=80%), the Brass-R texture {111}<112> is transformed into the Twinned-Copper texture {552} <115>[44]. Thus, Copper texture {112} <111> becomes very weak, and Brass-R texture {111} <112> is enhanced. Briefly, the Goss texture {110} <001>, Brass-R texture {111} <112>, Copper texture {112} <111>, and Twinned-Copper texture {552} <115> are generated during CR process.

When the as-rolled microstructures are recrystallized at 1120 °C, the recrystallization occurs in the deformed microstructures and the grains grow through the migration of grain boundaries. During the migration of grain boundaries, the coherent TBs are generated due to the accidentally disarranged stacking sequence by the (111) plane with atomic dense distribution. During TB migration, the annealing twins appear[9], which affects the orientation angle and leads to the texture transformation[11].

Fig.9 shows the texture variation of the as-rolled specimens after AT. When φ_2=0°, the Goss texture {110}<001>, Brass texture {110}<112>, and Brass texture {110}<110> appear along α orientation line. The Rotated-Cube texture {001}<110> and Cube texture {001}<100> appear along the θ orientation line. When φ_2=45°, the Brass-R texture {111}<112> and Brass texture {110}<112> exist along the γ orientation line. The Goss texture {110} <001>, Twinned-Copper texture {552}<115>, Copper texture {112}<111>, and Copper texture {112}<110> exist along the τ orientation line. In addition, the Cube texture {001}<100> and Cube texture {124}<211> appear when φ_2=65°.

The original grain has the recrystallization structure formed by solution treatment of the as-forged alloy. The recrystallized grains of AT specimens are formed by the recrystallization and grain growth of the deformed structures caused by AT. The grain orientation changes from anisotropy to isotropy. Compared with that of ST specimen, the Twinned-Copper

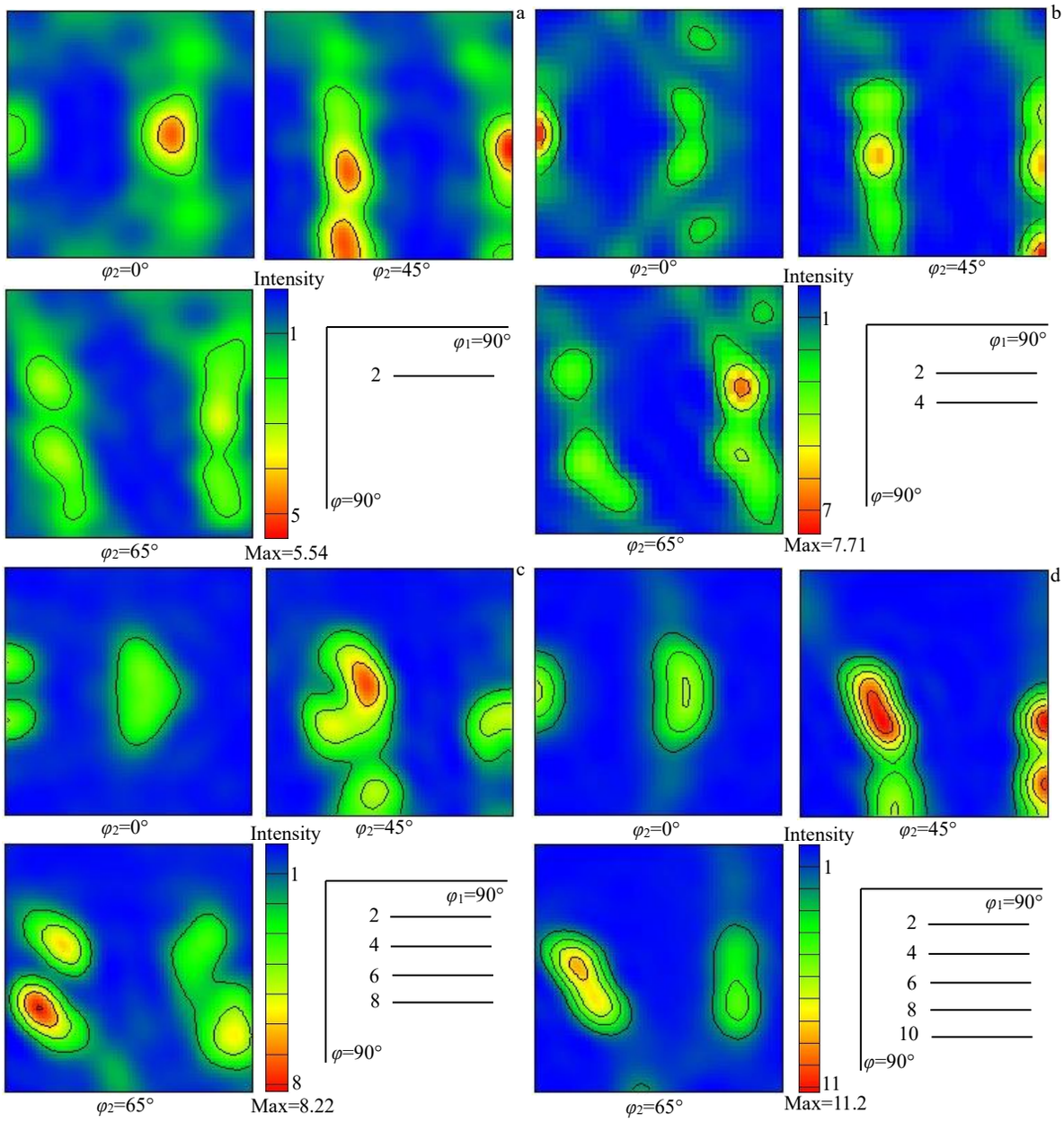

Fig.8 ODF sections of CR-30% (a), CR-45% (b), CR-70% (c), and CR-80% (d) Ni-based superalloys

texture {552}<115> is gradually enhanced, while the Goss texture {110}<001>, Brass texture {110}<112>, and Copper texture {112}<111> are gradually weakened. In addition, Cube texture {001}<100> and Cube texture {124}<211> appear on ODF section with φ_2=65°. This is because the twinning processes of the deformed microstructures during AT forms a large number of annealing twins. In addition, the unstable deformed grains are replaced by stable recrystallized grains, and thus the recrystallization texture appears, which increases the plastic deformation ability. The grains with recrystallization texture can easily form HAGBs, which leads to the merger between oriented grains and recrystallization texture through the migration of grain boundaries and preferential grain growth[43]. Besides, the recrystallized grains preferentially nucleate and grow due to the driving force provided by AT, which increases the growth tendency of the original oriented grains, and then the grains are coordinated and deformed. The texture {124}<211> also appears, which further enhances the annealed texture orientation and thereby improves the mechanical properties of the alloys[13].

Compared with those in CR specimens, the Rotated-Cube texture {001}<110>, Brass texture {110}<112>, Brass texture {110}<110>, Cube texture {001}<100>, Cube texture {112}<110>, and Cube texture {124}<211> are generated in the as-annealed specimens. The strength of Rotated-Cube texture {111}<112> and Goss texture {110}<001> weakens, while that of the Copper texture {112}<111> and Twinned-Copper texture {552}<115> is significantly improved. With increasing CR reduction, the Twinned-Copper texture

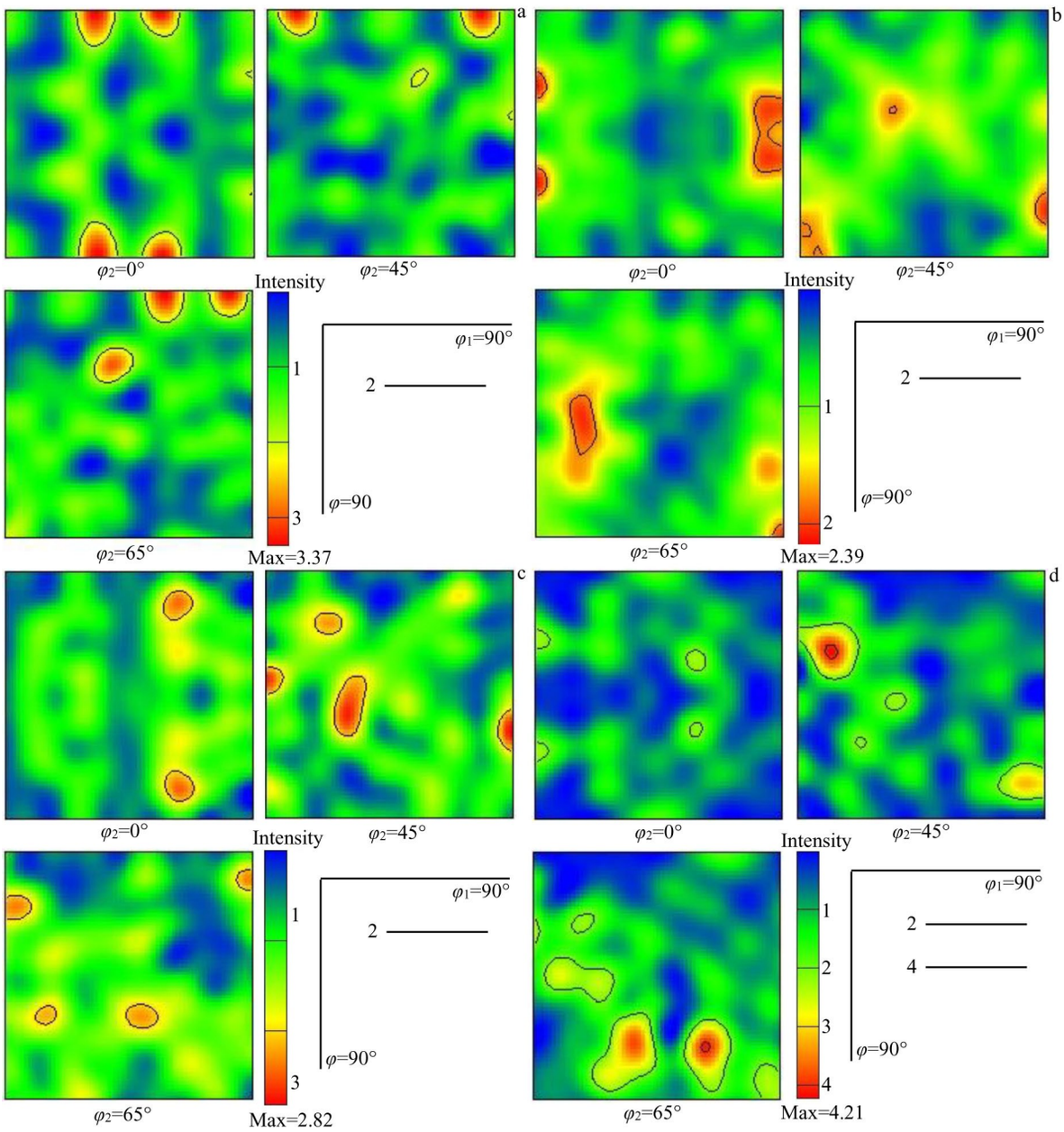

Fig.9 ODF sections of CR-30%-AT-1120-15 (a), CR-45%-AT-1120-15 (b), CR-70%-AT-1120-15 (c), and CR-80%-AT-1120-15 (d) Ni-based superalloys

{552} <115> in the as-annealed specimens is gradually enhanced, whereas other textures are weakened. This is because the storage energy is increased with increasing CR reduction. The driving force of recrystallization is different from that in the specimens subjected to different CR reductions[45], resulting in different proportions of annealing twins[46]. According to Fig. 3 and Fig. 5, with increasing CR reduction, the proportion of annealing twins is gradually increased: the proportion of annealing twins is 21.62%, 24.83%, 30.12%, and 46.42% when CR reduction is 30%, 45%, 70%, and 80%, respectively. The appearance of annealing twins continuously transforms the Copper texture {112}<111> into Twinned-Copper texture {552}<115>, and finally into Brass texture {110}<112>[24]. When the proportion of annealing twins increases, the strength of Copper texture {112}<111> decreases gradually and that of Twinned-Copper texture {552}<115> increases continuously. Furthermore, the {124}<211> texture appears due to the coordinated deformation of the grains during AT[25].

In conclusion, the recrystallization texture in the original grain provides a good plastic deformation condition for the alloy. The recrystallization texture is weakened, and the deformation texture is enhanced during CR treatment. After the subsequent AT process, a large number of annealing twins are produced due to the recrystallization, the deformation texture is weakened, and the Twinned-Copper texture {552}<115> is strengthened.

3 Conclusions

1) In the process of cold rolling (CR) deformation, the deformation degree affects the microstructure evolution of the Ni-based superalloy. When the CR reduction is small ($\varepsilon \leqslant$ 45%), the grains are elongated along the rolling direction into the flat shape and distributed uniformly. The crystals are mainly composed of low strain regions. However, the high strain regions are mainly distributed near the grain boundary. When the CR reduction exceeds 70%, the grain shape gradually changes from flat to fibrous, the deformation uniformity of the grain becomes better, and the strain distribution becomes more uniform.

2) In the Ni-based superalloys after CR and solid solution treatment, the sub-grain boundaries (Sub-GBs) and low angle grain boundaries (LAGBs) increase significantly, whereas the high angle grain boundaries (HAGBs) and twin boundaries (TBs) decrease significantly. With increasing CR reduction, LAGBs show an increasing trend. When the CR microstructure is annealed, the Sub-GBs act as the nucleation sites of new grains, and Sub-GBs and LAGBs begin to transform into HAGBs and TBs. In addition, TBs in the as-annealed alloy increase.

3) In the Ni-based superalloy after CR treatment, the microstructure contains Goss texture {110}<001>, Brass-R texture {111}<112>, Twinned-Copper texture {552}<115>, and Copper texture {112}<111>. With increasing the rolling deformation, the texture types do not change, but the texture strength is increased.

4) In the Ni-based superalloys treated by CR and annealing processes, many annealing twins are formed, which increases the texture types of in the alloys. Meanwhile, the appearance of annealing twins continuously transforms the Copper texture {112}<111> into Twinned-Copper texture {552}<115>, and finally into Brass texture {110}<112>. The strength of Copper texture {112}<111> is gradually weakened and that of the Twinned-Copper texture {552} <115> is continuously enhanced.

References

1 Du Jinhui, Lv Xudong, Dong Jianxin *et al. Acta Metallurgica Sinica*[J], 2019, 55(9): 1115 (in Chinese)

2 Wang Huiyang, An Yunqi, Li Chengyu *et al. Materials Reports*[J], 2011, 25(18): 482 (in Chinese)

3 Gu Yuefeng, Cui Chuanyong, Yuan Yong *et al. Acta Metallurgica Sinica*[J], 2015, 51(10): 1191 (in Chinese)

4 Zhang Beijiang, Huang Shuo, Zhang Wenyun *et al. Acta Metallurgica Sinica*[J], 2019, 55(9): 1095 (in Chinese)

5 Zhang Rui, Liu Peng, Cui Chengyong *et al. Acta Metallurgica Sinica*[J], 2021, 57(10): 1215 (in Chinese)

6 Heckl A, Neumeier S, Goken M *et al. Materials Science and Engineering A*[J], 2011, 528: 3435

7 Gao Yubi, Ding Yutian, Chen Jianjun *et al. Rare Metal Materials and Engineering*[J], 2020, 49(6): 1995 (in Chinese)

8 Qi Y W, Luo Z P, Li X Y *et al. Journal of Materials Science Technology*[J], 2022, 121: 124

9 Xia Shuang, Li Hui, Zhou Bangxin *et al. Chinese Journal of Nature*[J], 2010, 32(2): 94 (in Chinese)

10 Chen Jianjun, Ding Yutian, Wang Kun *et al. Acta Metallurgica Sinica*[J], 2021, 57(5): 641 (in Chinese)

11 Wang Zhongtang, Zhang Xiaoyu, Deng Yonggang *et al. Rare Metal Materials and Engineering*[J], 2014, 43(9): 2252 (in Chinese)

12 Wang Weiguo, Zhou Bangxin, Feng Liu *et al. Acta Metallurgica Sinica*[J], 2006, 42(7): 715 (in Chinese)

13 Han Ying, Yu Wei, Dong Entao *et al. Rare Metal Materials and Engineering*[J], 2021, 50(10): 3585 (in Chinese)

14 Fu X J, Lu J, Zhao Yan *et al. Rare Metal Materials and Engineering*[J], 2021, 50(8): 2721

15 Li Z S, Xiong Z H, Yang P *et al. Rare Metal Materials and Engineering*[J], 2022, 51(7): 2446

16 Liu Huan, Deng Siying, Song Hongwu *et al. Rare Metal Materials and Engineering*[J], 2021, 50(10): 3591 (in Chinese)

17 Guo Y N, Su H J, Yang P X *et al. Acta Metallurgica Sinica*[J], 2022, 35: 1407

18 Guo Y N, Su H J, Zhou H T *et al. Journal of Materials Science Technology*[J], 2022, 111: 298

19 Xia Shuang, Zhou Bangxin, Chen Wenjue*. Rare Metal Materials and Engineering*[J], 2008, 37(6): 999 (in Chinese)

20 Zheng Shijian, Yan Zhe, Kong Xiangfei *et al. Acta Metallurgica Sinica*[J], 2022, 58(6): 709 (in Chinese)

21 Wang X M, Ding Y T, Gao Y B *et al. Materials Science and Engineering A*[J], 2021, 823: 141 739

22 Gao Y B, Ding Y T, Ma Y J *et al. Materials Science and Engineering A*[J], 2021, 831: 142 188

23 Giannuzzi L A. *Materials Science and Engineering A*[J], 2000, 282(1): 270

24 Gao Yubi, Ding Yutian, Chen Jianjun *et al. Acta Metallurgica Sinica*[J], 2019, 55(4): 547 (in Chinese)

25 El-Danaf E, Kalidindi S R, Doherty R D *et al. Acta Materialia*[J], 2000, 48(10): 2665

26 Yuan Y, Gu Y F, Cui C Y *et al. Advanced Engineering Materials*[J], 2011, 13(4): 296

27 Chen J J, Ding Y T, Gao Y B *et al. Rare Metal Materials and Engineering*[J], 2021, 50(1): 14

28 Ding Yutian, Wang Xingmao, Meng Bin *et al. Chinese Journal of Rare Metals*[J], 2019, 43(3): 274 (in Chinese)

29 Ni Ke, Yang Yinhui, Cao Jianchun *et al. Acta Metallurgica Sinica*[J], 2021 57(2): 224 (in Chinese)

30 He Zhirong, Xie Niansuo, Zhang Yonghong. *Journal of Shaanxi Institute of Technology*[J]. 1996, 12(3): 1 (in Chinese)

31 Han Jihong, Zhang Yang, Ma Yaxi *et al. Materials Reports*[J], 2022, 36(24): 1 (in Chinese)

32 Mccarley J, Tin S. *Materials Science and Engineering A*[J], 2019, 740–741: 427

33 Pan Qingsong, Cui Fang, Tao Nairong *et al. Acta Metallurgica Sinica*[J], 2022, 58(1): 45 (in Chinese)
34 Zhou Ziqiang, Yue Xuelan, Huo Dengping. *Ordnance Material Science and Engineering*[J], 1998, 21(3): 3 (in Chinese)
35 Shih K K, Li J. *Journal of Materials Science*[J], 1976, 11: 1571
36 Gao X, Wu H B, Liu M *et al. Rare Metal Materials and Engineering*[J], 2021, 50(11): 3819
37 Li B L, Godfrey A, Meng Q C *et al. Acta Materialia*[J], 2004, 52(4): 1069
38 Randle V. *Scripta Materialia*[J], 2006, 54(6): 1011
39 Wang X M, Ding Y T, Yu H Y *et al. Materials Science and Engineering A*[J], 2022, 847: 143 293
40 Choi C H, Kwon J W, Oh E H *et al. Acta Materialia*[J], 1997, 45(12): 5119
41 Sidor J J, Kestens L A I. *Scripta Materialia*[J], 2013, 68(5): 273
42 Mao Weimin, Yang Ping, Chen Leng. *Material Texture Analysis Principle and Detection Technology*[M]. Beijing: Metallurgical Industry Press, 2008: 15 (in Chinese)
43 Hirsch J, Lvcke K. *Acta Metallurgica*[J], 1998, 36(11): 2883
44 Leffers T, Ray R K. *Progress in Materials Science*[J], 2009, 54(3): 351
45 Yu Lei, Luo Haiwen. *Acta Metallurgica Sinica*[J], 2020, 50(3): 291 (in Chinese)
46 Wu W R, Zhou Z, Sun H Z *et al. Rare Metal Materials and Engineering*[J], 2021, 50(6): 1971

镍基高温合金在变形热处理过程中的组织和织构演变

王 涛[1,2]，丁雨田[1,2]，王兴茂[1,2,3]，高钰璧[1,2]，毕中南[3]，杜金辉[3]，甘 斌[3]
(1. 兰州理工大学 省部共建有色金属先进加工与再利用国家重点实验室，甘肃 兰州 730050)
(2. 兰州理工大学 材料科学与工程学院，甘肃 兰州 730050)
(3. 钢铁研究总院 高温合金新材料北京市重点实验室，北京 100081)

摘 要：采用电子背向散射衍射技术研究了镍基高温合金冷变形和再结晶退火过程中的组织演变、晶界特征分布、应变分布及织构演变规律。结果表明，当冷变形量较小（ε≤45%）时，晶粒沿着轧制方向被拉长，呈扁平状于基体中均匀分布，应力主要集中在晶界和孪晶界（TB）附近，大角度晶界（HAGBs）和TBs逐渐向亚晶界（Sub-GBs）和小角度晶界（LAGBs）转变。同时，出现Goss织构{110}<001>、Brass-R织构{111}<112>、Twinned-Copper织构{552}<115>和Copper织构{112}<111>。当轧制压下量超过70%时，晶粒形状逐渐从扁平变为纤维状，晶粒的变形均匀性逐渐变好，应变分布变得均匀，LAGBs开始占主导地位。同时，织构类型保持不变，但织构强度增加。在1120 ℃退火15 min后，孪晶的长度分数随着轧制压下量的增加而增加。同时，变形织构转变为再结晶织构，织构类型增加，但织构强度减弱。此外，当退火孪晶的比例增加时，Copper织构{112}<111>不断向Twinned-Copper织构{552}<115>转变，并且经过30%~80%轧制变形的试样产生织构{124}<211>。

关键词：镍基高温合金；冷轧；退火孪晶；晶界特征分布；织构演变

作者简介：王 涛，男，1996年生，硕士生，兰州理工大学省部共建有色金属先进加工与再利用国家重点实验室，甘肃 兰州 730050，E-mail：just_wangtao@163.com